Soft Nanoparticle Crystals

DOI: 10.1002/anie.200904066

Probing in Real Time the Soft Crystallization of DNA-Capped Nanoparticles**

*Wenlong Cheng, Mark R. Hartman, Detlef-M. Smilgies, Rong Long, Michael J. Campolongo, Ruipeng Li, Karthik Sekar, Chung-Yuen Hui, and Dan Luo**

The crystallization of organically capped nanoparticles, unlike the hard-sphere crystallization of atoms, molecules, or conventional colloids, is a "soft process" in which the deformation of organic layers (soft coronae) unavoidably occurs. Despite previous efforts that focused mainly on structures at thermodynamic equilibrium,[1–11] it is not known how soft coronae deform dynamically in this soft-crystallization process. Here, using DNA-capped nanoparticles as a model system, we have probed in real time and in situ the entire drying-mediated soft-crystallization process by synchrotron-based small-angle X-ray scattering (SAXS). Notably, in our DNA-based approach[10,11] the known strategy of programmable crystal formation[12–14] is combined with drying-mediated self-assembly.[15] Our dynamic studies demonstrate that our soft crystals have continuously scalable crystalline states with a gradual transition from "wet crystals" to "dry crystals". We have found that the drying-mediated deformation of DNA molecules is elastic in accordance with an entropic spring model, which can also be applied in general to the drying-mediated self-assembly of other organically capped inorganic nanoparticles.

We define the softness of the soft-corona/solid-core particle by the dimensionless quantity $\chi = 2h_0/d_{core}$, where h_0 is the effective height of the corona layer and d_{core} is the diameter of the nanoparticle core (Figure 1). Compared to alkyl-chain-derivatized nanoparticles,[1–5,7] DNA-capped nanoparticles are much softer spheres. Based on our definition, we obtain a typical softness of 0.3–0.8 for alkyl-corona nanoparticles[16] and a softness of 0.6–5.1 for our DNA-corona nanoparticles (these consist of nanoparticles 13 nm in diameter end-grafted with single-stranded DNA (ssDNA) 5 to 90 bases in length). In contrast to the crystallization of colloidal hard spheres ($\chi = 0$), the drying-mediated stress that water imparts on the nanoparticles can lead to the deformation of soft-corona nanoparticles ($\chi > 0$). This stress is derived from surface tension, which increases with water evaporation.[17]

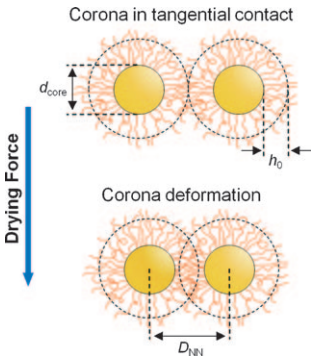

Figure 1. Representation of the deformation of soft-corona nanoparticles under drying forces. The soft-corona nanoparticles are inorganic nanoparticles (yellow spheres) end-grafted with extended-chain organic molecules. D_{NN} is the nearest-neighbor spacing, measurable by SAXS.

We mapped comprehensively (both temporally and spatially) the crystallization events of different DNA-capped nanoparticles over the entire lifetime of a drying droplet by means of real-time and in situ synchrotron-based SAXS. One-dimensional (1D) SAXS data (structure factor $S(q)$ versus scattering vector q; for details see the Supporting Information) was used to index crystalline lattices and quantitatively determine the nearest-neighbor spacing, D_{NN}. We first showed that nanoparticle supracrystals form for all DNA sequences investigated (see Section 1 in the Supporting Information), regardless of whether the sequences contain Watson–Crick base-pairing regions. However, the crystallization time, t_c, at which supracrystals start to form, varies between sequences. We compared time-lapse 2D SAXS images from the entire drying periods for 5′-TGTAC and

[*] Dr. W. L. Cheng, M. R. Hartman, M. J. Campolongo, K. Sekar, Prof. D. Luo
Department of Biological & Environmental Engineering
Cornell University, Ithaca, NY 14853 (USA)
Fax: (+1) 607-255-4080
E-mail: dan.luo@cornell.edu
wc272@cornell.edu
Homepage: http://luolabs.bee.cornell.edu
Dr. D.-M. Smilgies, Dr. R. Li
Cornell High Energy Synchrotron Source (USA)
R. Long, Prof. C.-Y. Hui
Department of Theoretical and Applied Mechanics
Cornell University (USA)
Dr. R. Li
National Synchrotron Radiation Laboratory
University of Science and Technology of China (P.R. China)

[**] We thank Dr. M. Kamperman and Prof. U. Wiesner for technical help and discussions as well as Prof. S. Gruner for critical reading of the manuscript. This work was supported in part by NYSTAR and a NSF CAREER award (grant no. 0547330). R.L. acknowledges a graduate student fellowship from the Chinese Scholarship Council. K.S. acknowledges the Cornell NBTC for financial support within the REU program. CHESS is supported by the NSF and the NIH/NIGMS through NSF award DMR-0225180. We also acknowledge the use of the facilities of the Cornell CCMR, which is supported through NSF grant DMR 0520404, part of the NSF MRSEC Program.
Supporting information for this article is available on the WWW under http://dx.doi.org/10.1002/anie.200904066.

5′-poly(dT)$_5$ (see online movies 1 and 2, respectively, in the Supporting Information). In online movie 1 (base-pairing), well-defined scattering rings are observed at the very beginning (a still image is shown in Figure 2a), demonstrating that

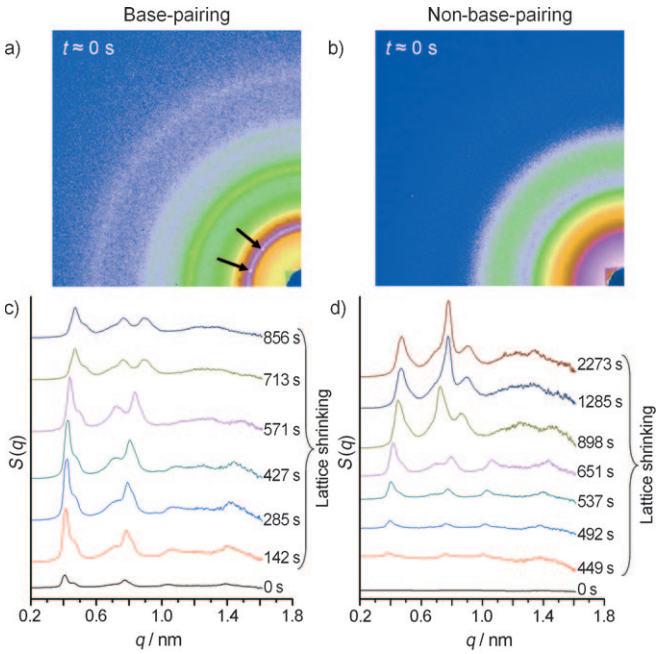

Figure 2. Soft crystallization of nanoparticles capped by 5′-TGTAC (a, c) and poly(dT)$_5$ (b, d). a,b) 2D detector images collected immediately after a droplet of the nanoparticle solutions had been positioned on the Kapton foil. Individual scattering spots are clearly observed in (a; see arrows). c,d) Series of 1D SAXS patterns recorded over drying time. In (d), the disproportionally large (220) peak in the later stage may have been caused by a preferential alignment of the crystallites induced by the Kapton foil substrate.

crystallization occurs at $t_c \approx 0$ s. Integration of the scattering rings leads to pronounced Bragg peaks in the 1D SAXS plot ($S(q)$ versus q; see the Supporting Information for details), which were indexed to a face-centered cubic (*fcc*) lattice (see Figure S2 in the Supporting Information). The lattice constant of the best-fit *fcc* unit cell is 26.1 nm, corresponding to a nearest-neighbor spacing, D_{NN}, of 18.5 nm. This value is consistent with the argument that the crystallization is triggered by specific Watson–Crick base-pairing and is in agreement with the results reported by Gang et al.[8] and Mirkin et al.[9]

In contrast, poly(dT)$_5$-mediated supracrystals (non-base-pairing) of the same initial concentration do not form at the beginning (Figure 2b) but form gradually in the intermediate stages of drying (see online movie 2 in the Supporting Information). At the initial stage of drying, the SAXS patterns exhibit diffuse scattering rings characteristic of form factors for noninteracting nanoparticles in dilute solution (Figure 2b). Upon evaporation of water from the drying droplet, the scattering intensity increases in response to the increasing nanoparticle concentration, but the overall lineshape does not change, until a certain concentration threshold is reached at the crystallization time t_c. Currently, we are unable to estimate the concentration threshold as nanoparticle concentrations vary inhomogeneously throughout the droplet (see online movie 3 in the Supporting information).

Regardless of the DNA sequences, supracrystals of DNA-capped nanoparticles exhibit continuously scalable crystalline states during water evaporation. We followed the development of 1D SAXS patterns after t_c for both base-pairing and non-base-pairing DNA-mediated supracrystals. We noticed that the overall scattering pattern remained after t_c but shifted to larger q values, which indicates lattice shrinkage (Figure 2c,d). Interestingly, the Bragg peaks in all of these 1D plots can be indexed to the *fcc* lattice, demonstrating that shrinkage of the lattice during soft crystallization is indeed uniform.

Unlike the 2D crystals formed in physically confined 2D films of water,[10] the crystals formed here are distributed inhomogeneously in three dimensions throughout the deposited droplets. We mapped the spatial distributions of crystallites within the deposited droplet by a raster scan of the whole droplet while the droplet was stabilized in a closed cell at 100% relative humidity. The results show that crystals are predominantly distributed in the contact-line regions with more pronounced crystalline events than in the center of the droplet (see Figure S3 in the Supporting Information). For the contact-line crystallization of poly(dT)$_{15}$-capped nanoparticles, the time-sequential 1D SAXS plots (Figure 3) clearly demonstrate a disorder–order transition (1→2) as well as the preservation of *fcc* superlattices (2→3→4) while the DNA coronae were being deformed by drying forces. The contact-

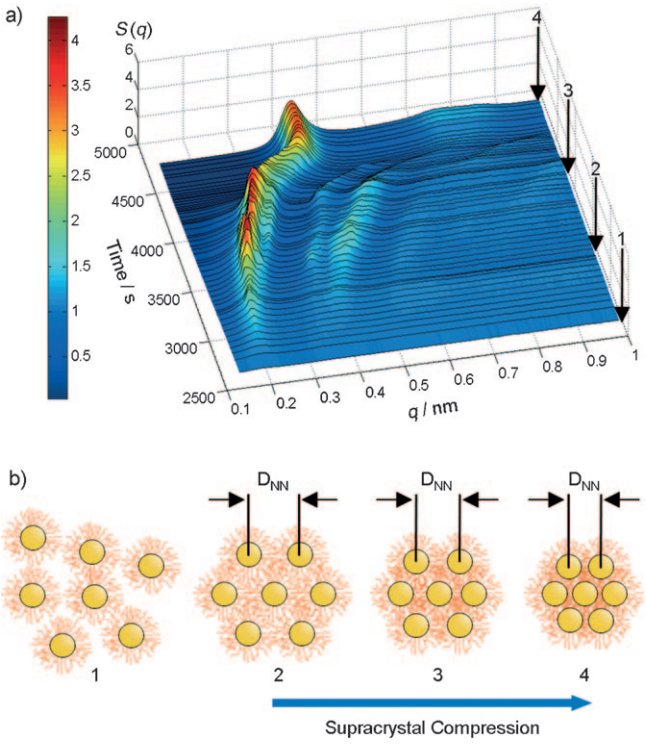

Figure 3. Soft crystallization of poly(dT)$_{15}$-capped nanoparticles in the contact-line region. a) Series of 1D SAXS patterns recorded over drying time; b) schematic showing the maintenance of the *fcc* lattice during corona deformation.

line crystallization events occurred in the regime in which D_{NN} ranges from $\approx$42.0 nm to $\approx$18.0 nm (see Figure S4a and online movie 4 in the Supporting Information), a much wider range than was observed in the center of the droplet (roughly 20.5 to 18.0 nm, see Figure S4b in the Supporting Information).

The wide range of the contact crystallization appears to be a result of the long-term maintenance of high local concentrations. It is known that the evaporation rate differs across a drop, with a higher rate at the contact line, which leads to outward capillary flow carrying solutes to the contact-line region.[18] The contact-line pinning leads to the "coffee ring" phenomenon. With an optical microscope, we observed that most of the nanoparticles indeed accumulate in the contact-line regions during the late stage of drying (see online movie 3 in the Supporting Information). The maintenance of the high local concentration significantly enhances entropy-driven crystallization.[19] We further show that faceted single supracrystals can be obtained from highly concentrated nanoparticle solutions (see Figure S5 in the Supporting Information).

Different from the reported pathway in which crystallization is driven by attractive base-pairing forces,[8,9,20–22] the drying-mediated crystallization of DNA-capped nanoparticles in this work is entropy driven. In the absence of Watson–Crick base-pairing forces, ssDNA-capped nanoparticles are highly repulsive (see Section 4 in the Supporting Information). Such repulsive spheres can crystallize only when the free volume is restricted to a certain threshold, which is similar to the case for conventional colloidal hard spheres.[23] The difference is that DNA-capped nanoparticles are soft spheres, hence, the resulting crystals are soft and shrinkable in response to the applied drying forces. In the soft-crystallization process, especially in the early stage of drying, core–core van der Waals forces may play a negligible role as particles are so far apart that their interparticle potential falls out of the van der Waals wells. Instead, ligand interactions are dominant[24,25] (possibly including van der Waals forces and nonspecific hydrogen bonding), which may help stabilize the dynamic crystals.

Previously, it has been demonstrated that DNA can widely regulate the lattice constants of crystals in the thermodynamic equilibrium states.[20,22,26] Here, we show that the dynamic lattice constants can also be widely tuned by adjusting DNA length. The softer nanoparticles (larger χ) crystallize over a wider dynamic regime (see Figure S6 in the Supporting Information). Within the limitation of our apparatus, we have observed dynamic crystallization within the range $\approx 20\text{ nm} < D_{NN} < \approx 50\text{ nm}$.

To further quantify soft crystallization, we established a theoretical model. The lattice shrinkage during soft crystallization suggests deformation of the corona. The corona must experience a transition from tangential contact to the equilibrium configuration of the fully dried state (Figure 1). We characterize the deformation of corona nanoparticles by defining a dimensionless deformation parameter [Eq. (1)],

$$\lambda = \frac{2h_0 - (D_{NN} - d_{\text{core}})}{2h_0 + d_{\text{core}}} \quad (1)$$

where D_{NN}, d_{core}, and h_0 are the nearest-neighbor spacing, diameter of nanoparticles, and original height of the non-deformed corona, respectively.

Consider a single nanoparticle with a corona under isotropic forces which lead to uniform deformation of the corona. Each single ssDNA chain is subjected to a compressive force f. Based on the entropic spring model of ideal polymer chains[27–30] and brush polymer theory,[27–30] we obtain Equation (2), where b, k_B, T, γ, and σ are the Kuhn length,

$$\lambda = \frac{2fb^{4/3}}{3k_BT(\gamma\sigma)^{1/3}}\frac{\chi}{1+\chi} \quad (2)$$

Boltzmann constant, temperature, scaling constant (including excluded volume effects), and the DNA strand number density per unit area of nanoparticle surface, respectively (see Section 2 in the Supporting Information). The parameters in our entropic spring model of the corona are experimentally measurable. The effective height of the ssDNA corona, h_0, was estimated by dynamic light scattering (see Table S3 in the Supporting Information,); the diameter of nanoparticle cores, d_{core}, was determined by a form factor simulation (Figure S1 in the Supporting Information) based on SAXS patterns from dilute solution; the nearest-neighbor spacing, D_{NN}, was obtained by SAXS.

The entropic spring model predicts that under the same force, the deformation parameter, λ, is solely dependent on the particle softness, χ. We compared the deformation of the corona nanoparticles in dried states by adjusting the softness, which is in agreement with our theoretical prediction (Figure 4a, black circles and solid line). The drying force applied to different corona nanoparticles is estimated to be about 16.6 nN. We further compared corona deformation for the free-standing nanoparticles superlattices,[10] which is also in agreement with our model (Figure 4a, blue circles and solid line). Nevertheless, the drying force in free-standing systems is smaller (about 15.3 nN) than that on the Kapton support. This is explained by the counteracting stress from the microhole edge which stretches the nanoparticle superlattice. We further note the generality of our spring corona theory which is also applicable to conventional alkyl-corona nanoparticles. The deformation data reported by Martin et al.[16] are reasonably well predicted by our spring model. Owing to the limited ligand length, alkyl-corona nanoparticles are stiffer and less compressible than our ssDNA-corona nanoparticles, and their deformation data exists only in the low χ region of the deformation curve (Figure 4a).

Based on our entropic spring model, we were able to estimate the temporal change of dynamic forces exerted on a single DNA chain. In the drying-mediated soft-crystallization process, the forces exerted on the DNA corona gradually increase (Figure 4b). The incremental increase in force leads to a smooth and uniform deformation of the DNA corona. Hence, a gradual shrinkage of supracrystals is observed in the dynamic crystallization process.

We further confirmed the springlike behavior of DNA coronae by demonstrating the reversibility of supracrystal deformation. By cycling between high and low relative humidity within a closed chamber, we observed a consequent

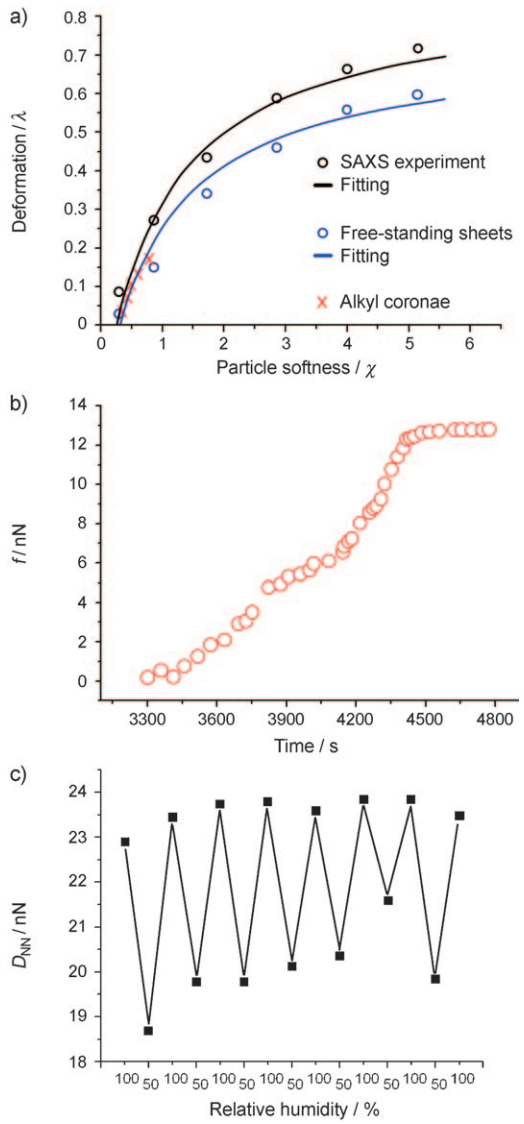

Figure 4. Springlike nature of the DNA corona. a) Correlation of the entropic spring model with experimental deformation. Black circles, blue circles, red crosses are DNA corona deformation values based on SAXS experiments on Kapton foils in this study, DNA-corona deformation values for free-standing superlattices from Ref. [10], and alkyl-corona deformation values from Ref. [16]. Black and blue solid lines are theoretical predictions based on our spring corona model. The fitting has included the drying effects, which account for a small deviation of experimental deformation values from theoretical calculations in ideal systems. b) The estimated drying forces applied to a DNA molecule during dynamic soft-crystallization. c) Changes in the nearest-neighbor spacing D_{NN} when the relative humidity is cycled between 50 and 100. Some salt (for example, 0.1 μL of 2 M NaCl) was added to the sample to increase the lattice shrinkage/expansion rates.

lattice expansion and shrinkage, respectively. Under low humidity, water molecules escape from the supracrystals. In this situation, forces exerted on DNA springs increase by means of water surface tension,[17] leading to corona contraction which results in a decrease of interparticle spacing. Under high humidity, water molecules in the vapor are absorbed by the supracrystals. This allows the DNA springs to relax and expand, thus increasing the interparticle spacing. We note that the supracrystal shrinkage/expansion behaviors were reversible over many cycles (Figure 4c), which opens a humidity-based route to regulate interparticle electromagnetic coupling interactions for applications in future adaptive nanodevices.

By means of synchrotron-based SAXS, we probed in real time and in situ the entire drying-mediated soft-crystallization process of DNA-capped nanoparticles. Our studies on dynamic crystallization demonstrated that DNA-mediated nanoparticle crystals are soft with continuously scalable crystalline states. In addition, we showed that crystallization time in the soft-crystallization process can be tuned by programming base-pairing forces. In particular, palindromic DNA sequences enabled crystallization events in the very beginning of the drying period, whereas non-base-paired poly(dT) sequences led to crystallization events at a much later stage of the drying process. Taking advantage of the fine and wide tunability of DNA molecular length, we investigated the softness-dependent crystallization process, which further allowed us to establish a general entropic spring model for the drying-mediated crystallization of soft-corona/solid-core nanoparticles.

We expect that the soft crystallization can be further tailored by engineering coronae mechanics; for example, building coronae with double-stranded DNA or branched DNA can potentially decrease softness.[31,32] Hence, we believe that soft-corona engineering will emerge as a promising route for the rational configuration and dynamic self-assembly of hard inorganic nanoparticles, which will ultimately lead to intelligent, adaptive nanoparticle-based devices.

Received: July 22, 2009
Revised: October 15, 2009
Published online: December 8, 2009

Keywords: crystal growth · DNA · nanoparticles · small-angle X-ray scattering

[1] C. P. Collier, T. Vossmeyer, J. R. Heath, *Annu. Rev. Phys. Chem.* **1998**, *49*, 371.
[2] R. L. Whetten, M. N. Shafigullin, J. T. Khoury, T. G. Schaaff, I. Vezmar, M. M. Alvarez, A. Wilkinson, *Acc. Chem. Res.* **1999**, *32*, 397.
[3] W. D. Luedtke, U. Landman, *J. Phys. Chem.* **1996**, *100*, 13323.
[4] B. A. Korgel, S. Fullam, S. Connolly, D. Fitzmaurice, *J. Phys. Chem. B* **1998**, *102*, 8379.
[5] C. J. Kiely, J. Fink, M. Brust, D. Bethell, D. J. Schiffrin, *Nature* **1998**, *396*, 444.
[6] A. K. Boal, F. Ilhan, J. E. DeRouchey, T. Thurn-Albrecht, T. P. Russell, V. M. Rotello, *Nature* **2000**, *404*, 746.
[7] A. M. Kalsin, M. Fialkowski, M. Paszewski, S. K. Smoukov, K. J. M. Bishop, B. A. Grzybowski, *Science* **2006**, *312*, 420.
[8] D. Nykypanchuk, M. M. Maye, D. van der Lelie, O. Gang, *Nature* **2008**, *451*, 549.
[9] S. Y. Park, A. K. R. Lytton-Jean, B. Lee, S. Weigand, G. C. Schatz, C. A. Mirkin, *Nature* **2008**, *451*, 553.
[10] W. L. Cheng, M. J. Campolongo, J. J. Cha, S. J. Tan, C. C. Umbach, D. A. Muller, D. Luo, *Nat. Mater.* **2009**, *8*, 519.
[11] W. L. Cheng, N. Park, M. T. Walter, M. R. Hartman, D. Luo, *Nat. Nanotechnol.* **2008**, *3*, 682.

[12] A. P. Alivisatos, K. P. Johnsson, X. G. Peng, T. E. Wilson, C. J. Loweth, M. P. Bruchez, P. G. Schultz, *Nature* **1996**, *382*, 609.
[13] C. A. Mirkin, R. L. Letsinger, R. C. Mucic, J. J. Storhoff, *Nature* **1996**, *382*, 607.
[14] U. Feldkamp, C. M. Niemeyer, *Angew. Chem.* **2006**, *118*, 1888; *Angew. Chem. Int. Ed.* **2006**, *45*, 1856.
[15] E. Rabani, D. R. Reichman, P. L. Geissler, L. E. Brus, *Nature* **2003**, *426*, 271.
[16] J. E. Martin, J. P. Wilcoxon, J. Odinek, P. Provencio, *J. Phys. Chem. B* **2000**, *104*, 9475.
[17] D. J. Trevor, *Handbook of Sol-gel Science and Technology*, *Vol. 3* (Ed.: S. Sakka), Kluwer Academic Publishers, Dordrecht, **2004**.
[18] R. D. Deegan, O. Bakajin, T. F. Dupont, G. Huber, S. R. Nagel, T. A. Witten, *Nature* **1997**, *389*, 827.
[19] O. D. Velev, *Science* **2006**, *312*, 376.
[20] H. M. Xiong, D. van der Lelie, O. Gang, *Phys. Rev. Lett.* **2009**, *102*, 015504-1.
[21] H. M. Xiong, D. van der Lelie, O. Gang, *J. Am. Chem. Soc.* **2008**, *130*, 2442.
[22] H. D. Hill, R. J. Macfarlane, A. J. Senesi, B. Lee, S. Y. Park, C. A. Mirkin, *Nano Lett.* **2008**, *8*, 2341.
[23] K. J. M. Bishop, C. E. Wilmer, S. Soh, B. A. Grzybowski, *Small* **2009**, *5*, 1600.
[24] U. Landman, W. D. Luedtke, *Faraday Discuss.* **2004**, *125*, 1.
[25] K. E. Mueggenburg, X. M. Lin, R. H. Goldsmith, H. M. Jaeger, *Nat. Mater.* **2007**, *6*, 656.
[26] R. J. Macfarlane, B. Lee, H. D. Hill, A. J. Senesi, S. Seifert, C. A. Mirkin, *Proc. Natl. Acad. Sci. USA* **2009**, *106*, 10493.
[27] P. G. De Gennes, *Scaling Concepts in Polymer Physics*, Cornell University Press, Ithaca, **1979**.
[28] D. Boal, *Mechanics of the Cell*, Cambridge University Press, Cambridge, **2002**.
[29] S. Alexander, *J. Phys.* **1977**, *38*, 977.
[30] P. G. de Gennes, *Macromolecules* **1980**, *13*, 1069.
[31] D. Luo, *Mater. Today* **2003**, *6*, 38.
[32] Y. G. Li, Y. D. Tseng, S. Y. Kwon, L. D'Espaux, J. S. Bunch, P. L. Mceuen, D. Luo, *Nat. Mater.* **2004**, *3*, 38.

